

ARTICLES

Rotational Relaxation in Supercritical CO₂[†]

John E. Adams* and Ali Siavosh-Haghighi

Department of Chemistry, University of Missouri-Columbia, Columbia, Missouri 65211-7600

Received: January 28, 2002; In Final Form: May 24, 2002

Though there are numerous studies of solute molecule rotational dynamics in ordinary liquids and supercritical fluids, few such studies have focused on the molecules of a neat supercritical fluid. In the present study, we investigate the structure and rotational dynamics of supercritical carbon dioxide at a temperature 1% above its critical temperature and over a 20-fold range of densities about the critical density. Our simulations reveal the presence of density inhomogeneities and thus regions of modest local density enhancement in this fluid over a significant range of bulk densities. Although these inhomogeneities account for the weak bulk density dependence of the CO₂ orientational correlation times in the near-critical regime, they are not reflected in a concomitant variation in the observed total rotational friction. Caution is warranted, however, in interpreting the usual diffusive dynamics parameters in this system because only at densities in excess of the critical density may the dynamics be characterized as diffusive; only at lower densities are orientational correlations found to decay on a time scale equal to or shorter than that characterizing the angular velocity correlations.

I. Introduction

Although in many instances, supercritical fluids have not proved to be the “super solvents” that they were once touted to be, they nonetheless afford an exceptionally versatile medium for the investigation of fundamental fluid properties.^{1–5} Their utility stems fundamentally from the fact that the density of a supercritical fluid (SCF) may be varied over a wide range without encountering a phase boundary. Consequently, density-dependent variations in the local structure of these fluids,^{4–19} and particularly the fluctuations that appear in the immediate vicinity of a solute molecule, have drawn considerable attention in the past fifteen years since Eckert²⁰ reported large negative partial molar volumes for naphthalene dissolved in near-critical ethane. Only recently, though, have definitive microscopic characterizations of a few model SCF solutions appeared, all of which have pointed to the presence of significant density inhomogeneities, especially when the system is near the critical point.^{14,17} For attractive solute–solvent systems, these density inhomogeneities in the cybotactic region are also found to extend well into the subcritical regime, suggesting a evolution from a potential-dominated local structure at low densities to a repulsion-dominated structure in the liquidlike regime.¹⁷ Yet the source of the observed inhomogeneities (specifically, local density enhancements) is not without controversy regarding the role of short-range attractive solute–solvent forces in determining the local solvent environment.^{21–27}

A full appreciation of the dynamics of a solute molecule requires that the solvent dynamics be fully characterized as well. Although a few noteworthy exceptions appear in the literature,^{28–37} wide-ranging systematic experimental investigations

of neat SCFs have not been actively pursued. The extant studies generally have considered only a few selected state points, and for the most part the points selected have been taken to lie well away from the critical point in order to avoid complications such as critical opalescence. Attempts at quantitative theoretical simulations of neat SCFs, on the other hand, have suffered from uncertainties regarding the phase diagrams corresponding to the assumed intermolecular forces.^{38–40} In most cases, studies have been carried out using potential functions for which the critical behavior is unknown or for which the critical parameters are well removed from the experimentally determined values. Thus, there remains a need for systematic studies of the density-dependent dynamics of these fluids.

The specific focus in the present work is on rotational relaxation dynamics.^{41,42} Because a molecule's rotation will be retarded by an effective friction deriving from the intermolecular interactions between the rotor and the surrounding molecules, a rotating molecule constitutes a sensitive probe of local fluid structure. An important limiting case obtains here when these interactions yield a sequence of uncorrelated, random collisions—this scenario describes the diffusive dynamical limit discussed by Debye.⁴³ But one also envisions a quite different dynamical limit, wherein the molecule essentially rotates freely over a time period that is of the order of the average time between molecular collisions. This second limiting case constitutes inertial (or “ballistic”) rotation. The time scale for the transition between these limiting behaviors will depend, of course, on the local collision frequency and hence on the local fluid density. Thus, by investigating how this time scale varies with a change in the bulk fluid density, one probes the extent to which the local density differs from that of the bulk fluid.

Carbon dioxide presents a particularly interesting system for the study of local density enhancements, in that it possesses no permanent dipole moment but nonetheless does have a large

[†] Part of the special issue “John C. Tully Festschrift”.

* To whom correspondence should be addressed. E-mail: AdamsJE@missouri.edu.

quadrupole moment, especially for a molecule of its size.⁴⁴ It also is a system for which we have a modest amount of experimental information about both fluid structure and rotational dynamics. Two decades ago Versmold extracted time-dependent reorientation information from depolarized Rayleigh scattering measurements performed for a 50-fold range of CO₂ densities.²⁹ Subsequent attempts to model these results over the entire range of densities have met with only limited success, although they have suggested that quadrupolar intermolecular interactions contribute significantly to the fluid's dynamical properties.^{38–40} (Quadrupolar forces can be important in solutions as well. Kauffman has shown recently that interactions between quadrupolar solvent molecules and a dipolar solute can accelerate certain isomerization reactions involving a charge transfer.^{45,46}) The experimental work on rotational relaxation dynamics is complemented by a series of neutron diffraction studies, most notably the recent ones of Cipriani et al.,^{47,48} that have added structural information to the emerging picture of fluid CO₂. These studies have yielded radial distribution functions (which necessarily include coherent neutron scattering amplitude weightings) that any theoretical model of this system minimally must reproduce.

In the present work, we describe molecular dynamics (MD) simulations of a neat CO₂ fluid carried out for a temperature near the critical temperature and over a wide range of densities. One of our primary interests here is in clarifying the conditions for which one may reasonably view the rotational dynamics as being fundamentally diffusive in character. Critical to this characterization is a determination of the relevant time scale for the ballistic rotation of CO₂ at the supercritical state points considered. By adopting a CO₂ intermolecular potential function that faithfully reproduces the location of the critical point,⁴⁹ we ensure that our results are directly comparable with those derived from experiments. A few of these results have already appeared in connection with our recent initial investigation of the dynamics of a toluene molecule dissolved in supercritical CO₂.¹⁹ The current study, however, expands significantly on that work and considers a wider range of fluid densities.

II. Simulations

The relevant dynamical quantities computed in this work are orientational and angular velocity correlation functions.⁴¹ Of the general form

$$C_{\ell}(t) = \langle P_{\ell}(\mathbf{u}(0) \cdot \mathbf{u}(t)) \rangle \quad (1)$$

the orientational functions reflect the time evolution of a unit vector \mathbf{u} lying along the CO₂ bond axis, the order ℓ of the Legendre polynomial being 1 if the result is to be compared with the results of infrared absorption experiments and 2 if the comparison is with Raman scattering or fluorescence depolarization results. In the limit of diffusive rotational dynamics, the family of orientational correlation functions is well represented by a simple exponential

$$C_{\ell}(t) \approx e^{-(\ell+1)D_{\text{R}}t} \quad (2)$$

and the rate at which orientational correlations are lost is well-characterized by a single rotational diffusion constant D_{R} . Note that in this limit, one predicts that there will be a simple relationship between the slopes of $\ln C_{\ell}(t)$ for different values of ℓ .

Complementing these quantities is the angular velocity correlation function

$$C_{\omega}(t) = \frac{\langle \boldsymbol{\omega}(0) \cdot \boldsymbol{\omega}(t) \rangle}{\langle |\boldsymbol{\omega}(0)|^2 \rangle} \quad (3)$$

which in the case of a linear molecule may be calculated about any axis lying perpendicular to the bond axis. (Note that this quantity is equivalent to the corresponding angular momentum correlation function because the moment of inertia factors cancel as a consequence of normalization.) Previous computational studies of rotational relaxation in liquids have found it convenient to focus on $C_{\omega}(t)$, because it generally decays on a shorter (and thus more accessible) time scale than do the corresponding orientational correlations.⁵⁰ However, as we will show below, this situation, which is characteristic of the Debye diffusive regime, does not obtain in supercritical CO₂ except at densities in excess of the critical density.

The CO₂ intermolecular potential function adopted in the present study is the EPM2 model devised by Harris and Yung,⁴⁹ which is of the all-atom, pairwise-additive Lennard–Jones form augmented with Coulombic terms, and which is scaled to yield the experimental critical parameters. The inclusion of Coulombic terms in this potential function appropriately builds quadrupole–quadrupole forces into the model. It is worth noting that the Harris–Yung EPM2 potential is identical in form to Jorgensen's all-atom OPLS potential,^{51,52} and accordingly the combining rules conventionally employed in the OPLS model are used here also.

All the results reported in the present work are based on sequences of canonical and microcanonical MD simulations carried out using Refson's *Moldy* code.⁵³ The system consisted of 1024 rigid CO₂ molecules confined to a cubic volume, the edge length of which was chosen so as to yield the desired bulk density. Initial atomic positions within that volume were selected using the "skew start" method implemented in *Moldy*, with randomly chosen initial molecular orientations. Full Ewald sums with conducting boundary conditions were employed in calculating long-range electrostatic contributions to the potential. An initial constant-*NVT* run of 20 ps was carried out to equilibrate the system at the chosen density (the selected step size was 0.002 ps and the temperature was fixed by periodic velocity rescalings), followed by a further run of 300 ps over which radial distribution functions were calculated. Correlation functions were then calculated on the basis of a series of 20, 10 ps constant-*NVE* simulations, the molecular position and velocity information being extracted from these runs at 0.04 ps intervals. (The first 4 ps of each 10 ps simulation yielded t_0 times used in the statistical averaging. Molecular translational and rotational velocities were rescaled prior to each constant-*NVE* simulation to restore the correct system temperature.)

III. Results

A. Radial Distribution Functions. As noted in the previous section, CO₂ radial distribution functions $g(r)$ were computed from system snapshots generated in constant-*NVT* simulations. Here, and throughout the present study, calculations were carried out for a system temperature that is 1% above the critical temperature ($T = 307$ K, $T_{\text{c}} = 304$ K). The carbon–carbon radial distribution functions, reflecting the distributions of molecular centers of mass, are shown in Figure 1 for a 20-fold range of system densities, from roughly $0.1\rho_{\text{c}}$ to $2\rho_{\text{c}}$ (the critical density ρ_{c} of CO₂ is $0.468 \text{ g}\cdot\text{cm}^{-3}$). At the lowest density considered, $g_{\text{C–C}}(r)$ is clearly gaslike, but with increasing bulk density, a smooth transition is made to a distinctly liquidlike form. Note that a clear demarcation of nearest-neighbor shells

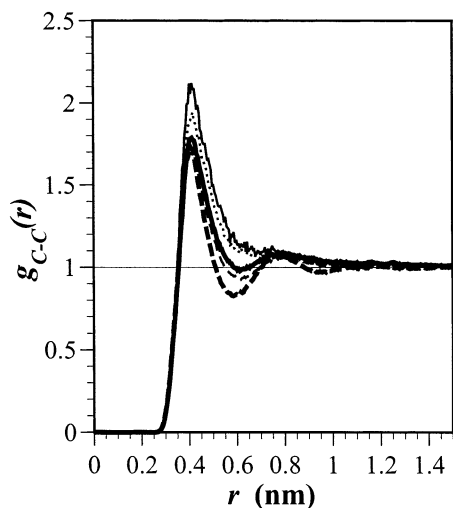


Figure 1. CO₂ radial distribution function for bulk densities of 0.0500 (thin solid line), 0.200 (dotted line), 0.468 (thick solid line), 0.600 (thin dashed line), and 1.000 (thick dashed line) g·cm⁻³ at a temperature of 307 K.

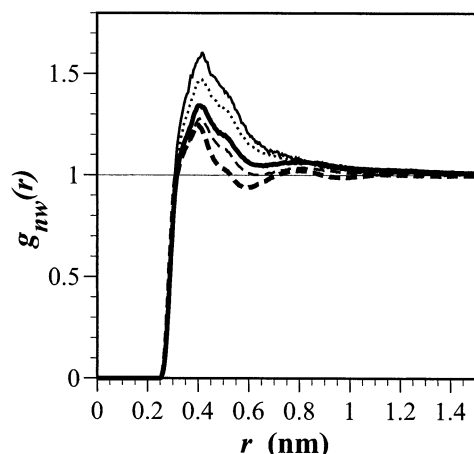


Figure 2. Neutron-weighted CO₂ radial distribution function for the same densities and temperature shown in Figure 1.

begins to appear in the vicinity of the critical density, where $g_{C-C}(r)$ passes through 1 at $r \approx 0.6$ nm.

Neutron scattering experiments do not yield $g_{C-C}(r)$ directly, of course, but rather they give a neutron-weighted distribution function $g_{nw}(r)$ that accounts for coherent neutron scattering from all of the atoms in carbon dioxide. As indicated by Cipriani et al.,⁴⁷ $g_{nw}(r)$ can be constructed from the various atom–atom distribution functions according to the relationship

$$g_{nw}(r) = 0.133g_{C-C}(r) + 0.464g_{C-O}(r) + 0.403g_{O-O}(r) \quad (4)$$

where the coefficients incorporate the coherent neutron scattering amplitudes of carbon and oxygen. Calculated $g_{nw}(r)$ curves, determined at the same five densities for which $g_{C-C}(r)$ is shown in Figure 1, are presented in Figure 2. One immediately finds features common to all of these neutron-weighted distribution functions: a main peak at $r = 0.4$ nm and two shoulders appearing in the region 0.33–0.35 nm and at 0.5 nm. (These shoulder features are largely attributable to maxima in $g_{O-O}(r)$ appearing at those positions.) Figure 3 shows a comparison of one of these $g_{nw}(r)$ with the most recent experimental findings,^{47,48} revealing a quite satisfactory agreement with respect both to the positions of the shoulders and to the peak heights. (Admittedly, the experiments were not done at precisely the

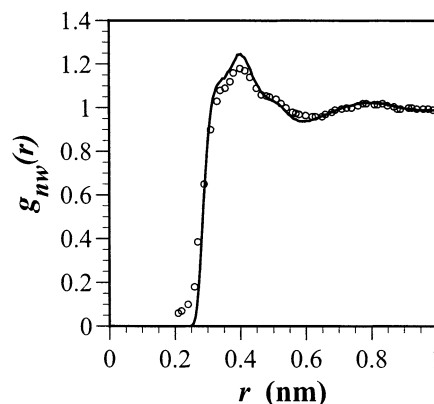


Figure 3. Neutron-weighted CO₂ radial distribution function calculated for $\rho = 1.000$ g·cm⁻³ (solid line) and the experimental results reported by Cipriani et al. (ref 48, open circles), which refer to $\rho = 0.83$ g·cm⁻³ and $T = 312$ K.

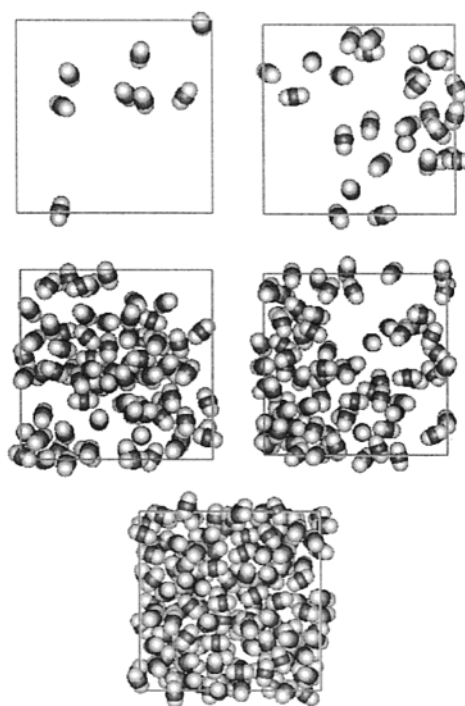


Figure 4. Snapshots of supercritical CO₂ for the densities (in increasing order, from left to right starting at the top) and temperature shown in Figure 1.

same thermodynamic state points as our calculations. Nonetheless, the dependence of the experimental curves on temperature and density have been found to be sufficiently weak that a direct comparison is still warranted.) It is also worth noting that our curves appear to agree as well or better than do the simulation results obtained by Cipriani et al.^{47,48} based on an all-atom Lennard-Jones plus point quadrupole potential model. (They found the inclusion of quadrupolar interactions to be essential for obtaining an acceptable agreement between the simulated and experimental distribution functions, especially for $R \leq 0.4$ nm.) Both their simulation results and ours slightly overestimate the height of the main $g_{nw}(r)$ peak while reproducing all the peak positions.

We turn now to a direct examination of characteristic snapshots of our system at various densities. In Figure 4 one finds orthoscopic projections of these snapshots, which include all molecules having one or more atoms lying within a $3.0 \times 3.0 \times 1.0$ nm volume that constitutes a subset of the full

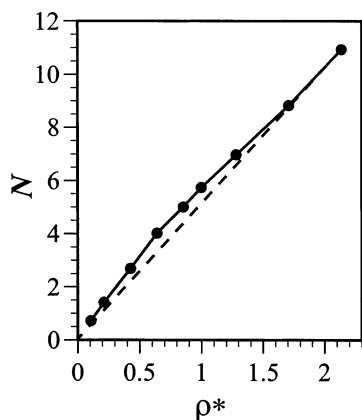


Figure 5. Calculated coordination numbers (solid points) as a function of reduced density, $\rho^* = \rho/\rho_c$. The dashed line is the result expected for a homogeneous mass distribution in the system.

simulation volume. (We present a fixed-volume subset of the full simulation volume here because the visual identification of any inhomogeneities is significantly more difficult in larger samples unless one is able to rotate the figure.) At the lowest density (top row, left) we see evidence for the formation of transient dimers and trimers, but the overall distribution of molecules is consistent with a gaslike state. Local density inhomogeneities become more pronounced, however, when one approaches half the critical density (top row, right); here one can see the preference for finding molecules in high-density regimes that has been reported by Tucker and co-workers¹⁴ in their two-dimensional SCF simulations. Increasing the system density to the critical density (middle row, left) increases the fraction of the total volume that may be deemed high-density, but voids are still observed and a fraction of the molecules are either in low-density regions or are on the boundary of a high-density region. This basic structure persists beyond the critical density as well; at $1.3\rho_c$ (middle row, right) the local environment appears to differ little from what is found at ρ_c . When the system is equilibrated at roughly twice the critical density (bottom row), however, we observe only the high-density (bulk) environment.

Although the system configuration snapshots are suggestive, a quantitative assessment of the density inhomogeneities is afforded by a calculation of local coordination numbers

$$N = 4\pi\rho \int_0^{r_1} dr r^2 g(r) \quad (5)$$

where the upper limit of the integral of the radial distribution function, r_1 , is taken as the position of the first minimum of $g(r)$ (which in the present case is just $g_{C-C}(r)$) in our highest-density results (i.e., at 0.59 nm). The local coordination numbers thus calculated are displayed in Figure 5, where the results attest to density enhancement in the subcritical and near-critical regimes. However, the enhancement is only modest, roughly 20% at most, reflecting the presence of no more than one additional solvent molecule in the first solvation shell.

B. Correlation Functions. As the local density increases, it takes progressively longer for a rotating molecule to move through any particular displacement angle, and thus the orientational correlation functions will decay on a longer time scale. This behavior in supercritical CO₂ is seen in the plots shown in Figures 6 and 7. In Figure 6, where $C_1(t)$ is given for a 20-fold range of densities, one sees that at the lowest densities this correlation function clearly departs from the exponential form characteristic of a system undergoing small diffusive angular

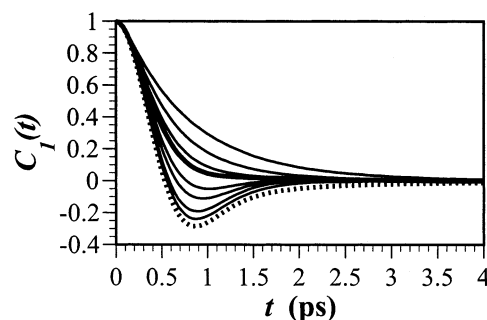


Figure 6. Orientational correlation function of CO₂ with $l=1$ at densities of 0.0500, 0.100, 0.200, 0.300, 0.468 (the critical density, thick line), 0.600, 0.800, and 1.000 g·cm⁻³. The dotted line is the corresponding free-rotor result described in the text.

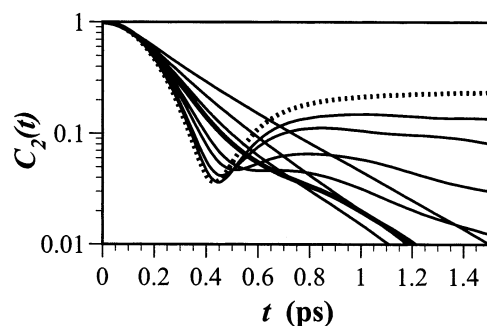


Figure 7. Orientational correlation function for CO₂ with $l=2$ at the densities shown in Figure 6.

displacements. In fact, at the lowest density studied (0.050 g·cm⁻³) $C_1(t)$ differs only slightly from the classical free-rotor result (the dotted line), obtained by (numerically) averaging the first Legendre polynomial over a Boltzmann distribution of rotational velocities.⁴² In all cases, the short-time behavior is quadratic, a result reflecting the fact that classical correlation functions are even functions of the time, but the onset of the departure from this initial quadratic behavior is clearly density-dependent. At the highest density studied (1.000 g·cm⁻³), the decay of $C_1(t)$ is well-represented by a single exponential at times greater than 0.2 ps with decay constant of 1.26 ps⁻¹. However, at $\rho = 0.800$ g·cm⁻³ the short-time quadratic influence is seen for times less than 0.6 ps, beyond which a single-exponential fit of the results yields a decay constant of 1.88 ps⁻¹. At lower densities, the fit to a single exponential is problematic — $C_1(t)$ decays sufficiently rapidly that contamination by computational “noise” complicates the fit, and indeed it is meaningless much below the critical density, where $C_1(t)$ is no longer positive-definite. Thus, only at the highest densities investigated do we find that the dynamics is consistent with a Debye model⁴³ of rotationally diffusive motion.

For the two highest densities noted above, determining a rotational relaxation time is reasonably straightforward. One is reminded, though, that there are several ways of making this determination, all of which derive from the assumption that $C_l(t)$ decays exponentially. For example, one may calculate the integral correlation time

$$\tau_l = \int_0^\infty C_l(t) dt \quad (6)$$

which should yield in this dynamical limit a result that is identical with the inverse of the decay constant obtained from a linear fit of $\ln C_l(t)$. The same result, in principle, may also be obtained by finding the time at which $C_l(t)$ decays to e^{-1} . Table 1 lists the calculated correlation times τ_1 for the entire

TABLE 1: Calculated Rotational Relaxation Times for Neat Supercritical CO₂

ρ (g·cm ⁻³)	ρ^*	τ_1 (ps)		τ_2 (ps)		τ_ω (ps)	
		integrated ^a	e^{-1b}	integrated	e^{-1}	integrated	e^{-1}
0.050	0.107	0.14	0.38	0.82	0.23	4.4	4.3
0.100	0.214	0.21	0.39	0.45	0.23	2.2	2.0
0.200	0.427	0.29	0.41	0.30	0.24	0.97	0.86
0.300	0.641	0.35	0.43	0.26	0.25	0.62	0.52
0.400	0.855	0.41	0.46	0.26	0.26	0.44	0.37
0.468	1.00	0.45	0.48	0.26	0.26	0.36	0.27
0.500	1.07	0.45	0.49	0.26	0.26	0.34	0.27
0.600	1.28	0.51	0.52	0.27	0.27	0.27	0.22
0.800	1.71	0.64	0.62	0.29	0.29	0.18	0.16
1.000	2.14	0.85	0.83	0.35	0.33	0.12	0.12
free rotor			0.37		0.23		

^a Relaxation time calculated by integration of the correlation function, eq 6. ^b Relaxation time equal to the time at which the value of the correlation function decays to e^{-1} .

range of densities investigated. Note that only at the higher densities is there good agreement between the two correlation times defined above and a fair agreement with the inverse of the fitted decay constant, the values of which for the densities 1.000 and 0.800 g·cm⁻³ are, respectively, 0.79 and 0.53 ps.

Also in Table 1 is τ_1 determined from the time at which the classical free-rotor correlation function (determined, as mentioned above, by means of numerical integration) takes on the value e^{-1} . Obviously, this value is not strictly a time constant for the decay of orientational correlations in an ensemble of unhindered rotors, since $C_1(t)$ is by no means exponential under these conditions. It nonetheless provides a useful time scale for characterizing unimpeded rotation. We note that there also is an alternate (analytical) specification of a free-rotor decay time as the time required for rotation with mean angular velocity of $(kT/I)^{1/2}$ (k being the Boltzmann constant and I the moment of inertia of CO₂, the latter equal to 7.015×10^{-45} kg·m² in the present model) through an angle of 68°. ^{54,55} (At this angle the averaged first Legendre polynomial, eq 1, falls to e^{-1} .)

$$\tau_{\text{FR}(1)} = (68/360)2\pi(kT/I)^{1/2} \quad (7)$$

This alternate approach leads to a free-rotor decay time for our system of 0.49 ps, a value that is on the order of 30% larger than the free-rotor τ_1 shown in Table 1.

Since the C_1 and C_2 correlation functions merely reflect two different ways of analyzing and depicting molecular reorientation dynamics, the trends observed in the calculated $C_1(t)$ curves carry over to the corresponding $C_2(t)$ curves. In Figure 7 we give logarithmic plots of the temporal dependence of C_2 , adopting the presentation format found in Versmold's description of his depolarized Rayleigh scattering experiments.²⁹ At densities greater than the critical density, the curves are characterized by a linear region at longer times, with the onset of this linear behavior, and thus of the simple exponential decay of C_2 , appearing at progressively shorter times as the density is increased. At lower densities two inflection points may be identified in each of the curves, the results approaching the corresponding free-rotor result (the dotted line), which exhibits a clear minimum at about 0.4 ps and an asymptotic value (the consequence of the functional form of the second Legendre polynomial) of 0.25.

Our calculated values of $C_2(t)$ are compared with selected experimental results of Versmold in Figure 8. A perfect agreement should not be expected here — the experimental results were obtained at a somewhat higher temperature (by 6 °C) and at different fluid densities than were ours. Nonetheless, the

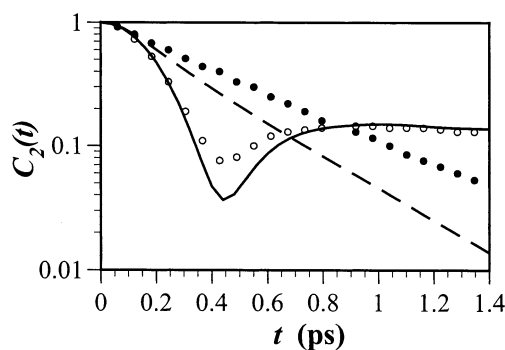


Figure 8. Calculated C_2 correlation functions for densities of 0.050 (solid line) and 1.000 (dashed line) g·cm⁻³. The experimental points reported by Versmold (ref 29) and shown for comparison purposes refer to densities of 0.042 (open circles) and 1.10 g·cm⁻³ (closed circles) and a temperature of 313 K.

agreement is good. For the two sets of low-density results, the minima in $C_2(t)$ appear at 0.40–0.45 ps, with a second maximum appearing at about 0.85 ps. Although the calculated values of C_2 are smaller than the corresponding experimental ones beyond 0.35 ps, the difference at the minimum is comparable to that found by Versmold when he compared his results to the values yielded by the J-diffusion model.⁵⁶ The two sets of high-density results, both of which reflect a linear time dependence of $\ln C_2(t)$, display significantly different slopes, but the variance is readily attributable to the difference in the system densities. Both our results and those of Versmold indicate that the magnitudes of the slopes of these $\ln C_2(t)$ curves in the high-density regime decrease as the density increases (translating, as shall be shown below, into a decrease in the rotational diffusion constant). Versmold's results, obtained at a density 10% higher than ours, are thus found appropriately to be characterized by a shallower slope. (At the risk of getting slightly ahead of ourselves in the data analysis, we can also extract rotational diffusion constants D_R from the slope of $\ln C_2(t)$ at long times. If we do so using our correlation functions calculated for the two highest densities and then extrapolate linearly to Versmold's highest system density, which is equivalent to 1.10 g·cm⁻³, we obtain a predicted D_R at that higher density of 0.43 ps⁻¹, which agrees well with the result 0.36 ps⁻¹ extracted directly from the reported experimental data.)

Correlation times derived from the temporal behavior of C_2 are given in Table 1. Again we find the (now expected) substantial difference at low densities between integral correlation times and those determined from the time at which C_2 decays to e^{-1} . While the latter times are a monotonically increasing function of fluid density, the integrated correlation function passes through a minimum in the vicinity of the critical density. (Exactly this same behavior was noted in the work of Okazaki et al. on supercritical fluoroform.²⁸) This behavior should not be considered surprising, given that in the free-rotor case, eq 6 yields an infinite value for τ_2 when C_2 does not asymptotically decay to zero. The corresponding free-rotor correlation time calculated assuming rotation with mean angular velocity $(kT/I)^{1/2}$, this time through an angle of 41°, ^{54,55} is now

$$\tau_{\text{FR}(2)} = (41/360)2\pi(kT/I)^{1/2} \approx (2\pi/9)(kT/I)^{1/2} \quad (8)$$

Under the conditions of our simulation, $\tau_{\text{FR}(2)} = 0.29$ ps, which again is somewhat larger than the one obtained from the temporal decay of C_2 . These results reinforce our previous remarks concerning the hazards implicit in interpreting correlation times in a dynamical regime that is manifestly nondiffusive, at least in the Debye sense.

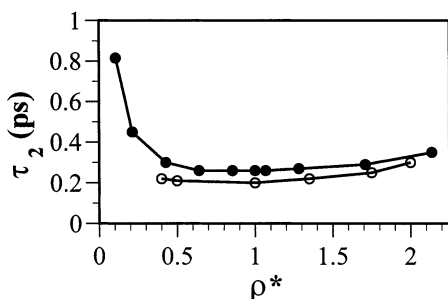


Figure 9. Orientational correlation times (τ_2) calculated in the present work (closed circles) and values extracted from NMR measurements by Holz et al. (ref 31, open circles).

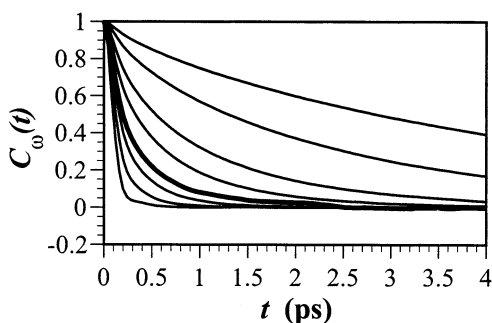


Figure 10. Angular velocity correlation function of CO₂ for the same densities shown in Figure 6.

The calculated τ_2 correlation times agree well with the times measured by Holz et al.³¹ in their study of ¹⁷O quadrupole relaxation rates by means of NMR. (Data extracted from that work is shown in Figure 9 along with our computed values.) Over a 4-fold density range the calculated and measured times vary by less than 30%. In contrast, the J-diffusion model^{56,57} results reported by Holz et al.³¹ overestimate the experimental correlation times by as much as 100% except at the highest densities examined, while at these high densities the predicted density dependence of the relaxation times is found to be qualitatively incorrect.

To elucidate the dynamics leading to the decay of the orientational correlation functions discussed above, we focus now on the angular velocity correlation function C_ω . As seen in Figure 10, the results are “inverted” with respect to those for C_χ in that it is now the least dense case that exhibits the slowest decay. (The free-rotor case here is trivial— $C_\omega(t)$ is unity for all t in the absence of collisions that perturb the rotational velocity.) One is struck here by the much stronger dependence on density of the time scale over which the angular velocity correlations decay in comparison with what was found in the case of C_χ . Quantitation of this observation is possible by calculating the correlation times in a fashion exactly analogous with the determination of τ_χ . The results of these calculations, given in Table 1, indicate that a 20-fold increase in density is associated with, roughly, a 40-fold decrease in the correlation time. (Here the two methods of calculating τ_ω yield similar results over the entire density range, even though both derive from an assumed a simple exponential temporal dependence of C_ω , whereas in fact at short times the correlation function is necessarily quadratic in the time.^{41,42}) These values also provide insight into the dynamics of supercritical CO₂ when they are compared to the corresponding orientational correlation times. In Figure 11 we provide a plot of the integral correlation time data, which shows that only for densities in excess of about 0.6 g·cm⁻³ do both orientational correlation times exceed the angular velocity correlation time. The significance of this result becomes clear

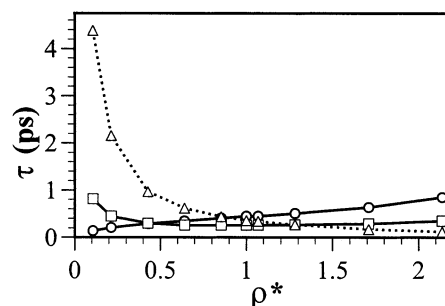


Figure 11. Integral correlation times, eq 6, for angular orientation ($l = 1$, circles; $l = 2$, squares) and angular velocity (triangles). (The connecting lines are shown merely to guide the eye.) Density here is in reduced units, $\rho^* = \rho/\rho_c$.

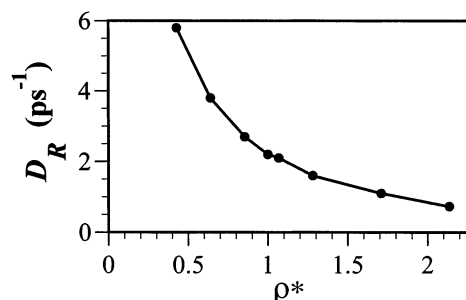


Figure 12. Rotational diffusion constants, eq 9, as a function of reduced density, $\rho^* = \rho/\rho_c$.

when one examines a fundamental assumption of the diffusive dynamical model, namely that velocity correlations decay more rapidly than do the orientational correlations. Thus, we are strictly justified in defining decay times in this system at $T = 1.01T_c$ only when the bulk density is on the order of 130–150% of the critical density.

The rotational diffusion constant can be determined from the same information as the angular velocity correlation function

$$D_R = \int_0^\infty \langle \omega(t)\omega(0) \rangle dt \quad (9)$$

Values calculated using this formula are displayed in Figure 12. The density dependence of D_R seen there is, as one would expect from a comparison of eqs 6 and 9, the same as we found for τ_ω — D_R is approximately inversely proportional to ρ , at least in the subcritical and near-critical regime. One must, of course, be cautious in interpreting these results, given the conclusions drawn from the results presented in Figure 11, namely that the rotational motion is diffusive (in the Debye sense) only at the highest densities investigated. Nonetheless, the calculated values point to an increasing perturbation of the molecule's angular velocity with increasing bulk density.

Equation 2 also provides a means for calculating D_R in the diffusive dynamical regime, a plot of $\ln C_l(t)$ versus time should be linear with a slope equal to $-(l+1)D_R$. At the highest density considered (1.000 g·cm⁻³), such a plot of $\ln C_1(t)$ yields a rotational diffusion constant of 0.63 ps⁻¹, whereas a plot of $\ln C_2(t)$ yields the value 0.51 ps⁻¹. (The ratio of the slopes of these two lines is 2.4, and thus is within 20% of the theoretical value of 3.0.) The average of these two results is 0.57 ps⁻¹, which itself agrees reasonably well with the value calculated by integration of the angular velocity correlation function, eq 9, although the result obtained from the long-time behavior of $C_1(t)$ is in better agreement. (This latter number is the “asymptotic” value for D_R shown in Table 1.) At a bulk density of 0.800 g·cm⁻³, the corresponding values obtained from the

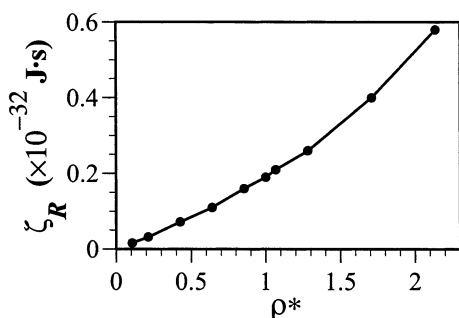


Figure 13. Total rotational friction as a function of reduced density, $\rho^* = \rho/\rho_c$.

asymptotic behavior of the C_1 and C_2 correlation functions are 0.94 and 0.67 ps⁻¹, respectively, and the ratio of the slopes as discussed above is now only 2.2. Again, however, the $C_1(t)$ data provides an estimate of D_R comparable with that obtained from $C_\omega(t)$. At lower densities this agreement deteriorates, but such an outcome is hardly surprising given the significant departure from strictly exponential behavior at these densities exhibited in Figures 6 and 7.

In Figure 13 we display values of the total (zero-frequency) rotational friction coefficient,⁴² which in the diffusive limit is given by the Einstein relation

$$\zeta_R = kT/D_R \quad (10)$$

and thus is inversely proportional to the corresponding rotational diffusion constant value. The bulk density dependence of ζ_R appears to be nearly linear for $\rho \leq \rho_c$. Beyond this range, though, where the dynamics is more strictly diffusive, a higher-order dependence of the total friction on density becomes apparent.

Even acknowledging the limits on the range of validity of eq 10, one naturally wonders why the calculated density dependence of ζ_R does not manifest the signature of local density enhancement that might be expected, even for the modest density enhancements calculated for CO₂. Indeed, the weak bulk density dependence of τ_2 over the range of densities for which local density enhancement is observed (see Figures 5 and 9) makes the results shown in Figure 13 particularly surprising. Our findings are by no means unique, however. A very recent study of solute friction in supercritical CO₂ carried out by Maroncelli and co-workers⁵⁸ has suggested that local density enhancement can be "hidden" as a consequence of an interesting cancellation of effects: the amplitude of the friction, which reflects repulsive intermolecular interactions and *does* mirror density augmentation, is offset by a variation of the correlation time of the friction. The net result is that a supercritical fluid, even though it may be characterized by significant density inhomogeneities, exhibits a total friction that is appropriate to a "normal" liquid. (The linear density dependence of the total friction seen in Figure 13 is, for example, consistent with an Enskog model,⁵⁹ which predicts that the total friction will scale as the density multiplied by the value of the radial distribution function at contact. Because the latter function is not changing significantly over the density range considered in this work, the linear dependence on ρ dominates the overall result.) The present results thus lend support to their speculation that the insensitivity of the total friction to local variations in the fluid density may be a general characteristic of the supercritical regime.

IV. Concluding Remarks

We have carried out simulations of supercritical carbon dioxide over a 20-fold range of densities along an isotherm that

is 1% above the critical temperature. The results of these calculations are consistent with an inhomogeneous distribution of mass in the neat nondipolar fluid and, thus, with a propensity for molecules to be found in environments characterized by an enhanced local density. At the same time, our calculations indicate that the total rotational friction and the corresponding diffusion constant are poor probes of such enhancement. In interpreting these results, though, it must be remembered that only at densities beyond the critical density may the rotational dynamics in the present system truly be viewed as diffusive (at least in the Debye sense) and thus be described accurately by exponentially decaying correlation functions.

The present results are relevant also to dilute solutions of solutes whose net interactions with carbon dioxide are attractive. Such species necessarily will tend to be found in regions of locally high CO₂ density, and thus they will exhibit a shift in their properties of a magnitude appropriate to solvation in a fluid of higher bulk density. This behavior indeed is what was seen in the two-dimensional simulations reported by Tucker and co-workers.¹³ Note that the physical model suggested by the present work does not require that local density enhancement be solute-induced in the near-critical regime, a degree of solute inhomogeneity exists even in the absence of a solute. On the other hand, local density enhancements beyond those seen in the neat fluid would be suggestive of solute-induced structure.

Acknowledgment. The authors are pleased to acknowledge several useful discussions with J. Kauffman concerning the present work, as well as particularly thoughtful and helpful comments from an anonymous referee. This article is dedicated to John Tully in recognition of his many important contributions to the understanding of molecular dynamics.

References and Notes

- Jang, J.; Stratt, R. M. *J. Chem. Phys.* **2000**, *112*, 7524.
- Jang, J.; Stratt, R. M. *J. Chem. Phys.* **2000**, *112*, 7538.
- Reynolds, L.; Gardecki, J. A.; Frankland, S. J. V.; Horng, M. L.; Maroncelli, M. *J. Phys. Chem.* **1996**, *100*, 10 337.
- Kajimoto, O. *Chem. Rev.* **1999**, *99*, 355.
- Tucker, S. C. *Chem. Rev.* **1999**, *99*, 391.
- Biswas, R.; Lewis, J. E.; Maroncelli, M. *Chem. Phys. Lett.* **1999**, *310*, 485.
- Heitz, M. P.; Maroncelli, M. *J. Phys. Chem. A* **1997**, *101*, 5852.
- Song, W.; Biswas, R.; Maroncelli, M. *J. Phys. Chem. A* **2000**, *104*, 6924.
- Egorov, S. A. *J. Chem. Phys.* **2000**, *112*, 7138.
- Egorov, S. A. *J. Chem. Phys.* **2000**, *113*, 1950.
- Egorov, S. A.; Yethiraj, A.; Skinner, J. L. *Chem. Phys. Lett.* **2000**, *317*, 558.
- Adams, J. E. *J. Phys. Chem. B* **1998**, *102*, 7455.
- Goodyear, G.; Maddox, M. W.; Tucker, S. C. *J. Chem. Phys.* **2000**, *112*, 10 327.
- Goodyear, G.; Maddox, M. W.; Tucker, S. C. *J. Phys. Chem. B* **2000**, *104*, 6258.
- Goodyear, G.; Maddox, M. W.; Tucker, S. C. *J. Phys. Chem. B* **2000**, *104*, 6240.
- Maddox, M. W.; Goodyear, G.; Tucker, S. C. *J. Phys. Chem. B* **2000**, *104*, 6266.
- Maddox, M. W.; Goodyear, G.; Tucker, S. C. *J. Phys. Chem. B* **2000**, *104*, 6248.
- Tucker, S. C.; Maddox, M. W. *J. Phys. Chem. B* **1998**, *102*, 2437.
- Siavosh-Haghighi, A.; Adams, J. E. *J. Phys. Chem. A* **2001**, *105*, 2680.
- Eckert, C. A.; Ziger, D. H.; Johnston, K. P.; Kim, S. *J. Phys. Chem.* **1986**, *90*, 2738.
- Cherayil, B. J.; Fayer, M. D. *J. Chem. Phys.* **1997**, *107*, 7642.
- Myers, D. J.; Chen, S.; Shigeiwa, M.; Cherayil, B. J.; Fayer, M. D. *J. Chem. Phys.* **1998**, *109*, 5971.
- Urdahl, R. S.; Rector, K. D.; Myers, D. J.; Davis, P. H.; Fayer, M. D. *J. Chem. Phys.* **1996**, *105*, 8973.
- Myers, D. J.; Shigeiwa, M.; Cherayil, B. J.; Fayer, M. D. *J. Chem. Phys.* **2001**, *115*, 4689.

- (25) Myers, D. J.; Shigeiwa, M.; Stromberg, C.; Fayer, M. D.; Cherayil, B. *J. Chem. Phys. Lett.* **2000**, 325, 619.
- (26) Myers, D. J.; Shigeiwa, M.; Fayer, M. D.; Cherayil, B. *J. Phys. Chem. B* **2000**, 104, 2402.
- (27) Ruckenstein, E.; Shulgin, I. *J. Phys. Chem. B* **2000**, 104, 2540.
- (28) Okazaki, S.; Matsumoto, M.; Okada, I. *J. Chem. Phys.* **1995**, 103, 8594.
- (29) Versmold, H. *Mol. Phys.* **1981**, 43, 383.
- (30) Zhou, Y.; Constantine, S.; Harrel, S.; Gardecki, J. A.; Ziegler, L. D. *J. Raman Spectrosc.* **2000**, 31, 85.
- (31) Holz, M.; Haselmeier, R.; Dyson, A. J.; Huber, H. *Phys. Chem. Chem. Phys.* **2000**, 2, 1717.
- (32) Ishii, R.; Okazaki, S.; Okada, I.; Furusaka, M.; Watanabe, N.; Misawa, M.; Fukunaga, T. *Chem. Phys. Lett.* **1995**, 240, 84.
- (33) Saitow, K. i.; Ohtake, H.; Sarukura, N.; Nishikawa, K. *Chem. Phys. Lett.* **2001**, 341, 86.
- (34) Saitow, K.-i.; Ochiai, H.; Kato, T.; Nishikawa, K. *J. Chem. Phys.* **2002**, 116, 4985.
- (35) Nishikawa, K.; Takematsu, M. *Chem. Phys. Lett.* **1994**, 226, 359.
- (36) Nishikawa, K.; Tanaka, I. *Chem. Phys. Lett.* **1995**, 244, 149.
- (37) Nishikawa, K.; Tanaka, I.; Amemiya, Y. *J. Phys. Chem.* **1996**, 100, 418.
- (38) Böhm, H. J.; Meissner, C.; Ahlrichs, R. *Mol. Phys.* **1984**, 53, 651.
- (39) Singer, K.; Taylor, A. J.; Singer, J. V. L. *Mol. Phys.* **1977**, 33, 1957.
- (40) Singer, K.; Singer, J. V. L.; Taylor, A. J. *Mol. Phys.* **1979**, 37, 1239.
- (41) Berne, B. J.; Harp, G. D. In *Advances in Chemical Physics*; Prigogine, I., Rice, S. A., Eds.; Wiley: New York, 1970; Vol. 17; p 63.
- (42) Hansen, J. P.; McDonald, I. R. *Theory of Simple Liquids*, Second ed.; Academic Press: London, 1986.
- (43) Debye, P. *Polar Molecules*; Dover: New York, 1945.
- (44) Buckingham, A. D.; Disch, R. L. *Proc. R. Soc. A* **1963**, 273, 275.
- (45) Khajepour, M.; Kauffman, J. F. *J. Phys. Chem. A* **2000**, 104, 9512.
- (46) Kauffman, J. F. *J. Phys. Chem. A* **2001**, 105, 3433.
- (47) Cipriani, P.; Nardone, M.; Ricci, F. P. *Nuovo Cimento Soc. Ital. Fis., D* **1998**, 20D, 1147.
- (48) Cipriani, P.; Nardone, M.; Ricci, F. P. *Physica B (Amsterdam)* **1998**, 241–243, 940.
- (49) Harris, J. G.; Yung, K. H. *J. Phys. Chem.* **1995**, 99, 12 021.
- (50) Kurnikova, M. G.; Waldeck, D. H.; Coalson, R. D. *J. Chem. Phys.* **1996**, 105, 628.
- (51) Jorgensen, W. L.; Tirado-Rives, J. *J. Am. Chem. Soc.* **1988**, 110, 1657.
- (52) Jorgensen, W. L.; Briggs, J. M.; Contreras, L. *J. Phys. Chem.* **1990**, 94, 1683.
- (53) Refson, K. *Comput. Phys. Commun.* **2000**, 126, 310.
- (54) Bartoli, F. J.; Litovitz, T. A. *J. Chem. Phys.* **1972**, 56, 413.
- (55) Bauer, D. R.; Brauman, J. I.; Pecora, R. *J. Am. Chem. Soc.* **1974**, 96, 6840.
- (56) Gordon, R. G. *J. Chem. Phys.* **1966**, 44, 1830.
- (57) Powles, J. G.; Rickayzen, G. *Mol. Phys.* **1977**, 33, 1207.
- (58) Patel, N.; Biswas, R.; Maroncelli, M. *J. Phys. Chem. B*, submitted.
- (59) McQuarrie, D. A. *Statistical Mechanics*; Harper & Row: New York, 1976; p 530.